PFC/RR-87-16 DOE/ET-51013-230
UC20,d,f

Suitability of Millimeter-Wave Scattering for Diagnostics of Fusion Alpha-Particles

P. P. Woskov*

September 1987

Plasma Fusion Center
Massachusetts Institute of Technology
Cambridge, MA

*Formerly P. Woskoboinikow

ABSTRACT

Collective Thomson scattering using long-pulse, millimeter-wave sources is potentially a powerful diagnostic technique of localized alpha particle velocity distribution and density in a fusion tokamak. The combination of a long-pulse and long-wavelength source optimizes the achievable signal to noise ratio of this diagnostic. Additional advantages of millimeter-waves include large scattering angles up to 180°, wide-bandwidth receivers, and suitability of millimeter waveguide techniques in a radiation environment. The Doppler broadened scattered spectrum provides an unambiguous measure of the alpha particle parameters even for a scattering plane orientation near perpendicular to the magnetic field because magnetized particle resonances will be averaged out by finite diagnostic beam divergence and frequency resolution. Millimeter-wave accessibility in tokamaks using x-mode propagation at frequencies between the lower x-mode cutoff and the upper hybrid resonance may be a natural consequence of high field tokamak operation.

Contents

1. INTRODUCTION

Diagnostics of energetic, confined fusion ion products will be important for the study of ignition tokamak physics. Power deposition by these fusion products is expected to sustain an ignited plasma burn. However, many questions have been raised as to how this heating power will impact the tokamak plasma parameters. In the first D-T burning tokamaks 3.5 MeV alpha particles ($^4He^{++}$) will be produced. Alpha particle density, velocity distribution, and induced instabilities will need to be diagnosed with both spatial and temporal resolution.

Several recent workshops and reviews [1-4] have dealt with the subject of alpha particle diagnostics. Most proposed confined alpha diagnostics can be catagorized either as a technique which depends on a particle interaction such as a nuclear reaction or a single or double charge exchange, or as an electromagnetic wave technique such as ion cyclotron emission or collective Thomson scattering. Each of these proposed diagnostics has its strengths and weaknesses. The criteria for choosing which to develop will depend on the quality of information that the diagnostic can provide, its potential for working, and its suitability for the environment of the tokamak device. In this paper the case for collective Thomson scattering using long-pulse millimeter waves will be presented.

1.1 Collective Thomson Scattering

The signals generated by a collective Thomson scattering diagnostic can provide a good measure of the alpha particle parameters. High-power electromagnetic radiation is scattered by the Debye shielding electron clouds moving with the plasma ions. Direct scattering by the ions is not significant because a charged particle's scattering cross section is inversely proportional to the square of its mass. Nevertheless, the scattered frequency spectrum is Doppler broadened due to the ion velocities. The alpha particles, being the fastest ions, will cause the largest Doppler shift. Detecting the shape and signal level of this scattered spectrum can therefore provide an unambiguous measurement of the alpha particle velocity distribution and density.

There are several additional advantages inherent in this diagnostic technique. Good spatial resolution is possible because the scattered signal is localized to the intersection of the electromagnetic beam and the detection field of view. Good time resolution on the order of a microsecond is possible; however, longer millisecond time scales can provide significant signal to noise ratio margins as described below. Finally, the measurement is nonperturbing. Practical diagnostic beam intensities ($<<10$ GWcm^{-2}) are not sufficiently powerful to accelerate plasma electrons significantly relative to their thermal velocity.

There is a good historical basis for this diagnostic as well. Since the late 1950's the ion temperature, ionic composition, and other plasma parameters in the earth's ionosphere have been studied using high-power radar back-scattering [5,6]. Since the mid 1960's similar measurements have been made in theta pinch and arc plasmas using visible [7,8] and 10μm CO_2 lasers [9,10], and finally, in the 1980's the feasibility of applying this diagnostic to tokamaks was demonstrated on

Alcator C and TCA using 385μm D_2O lasers [11,12]. The theoretical basis for this diagnostic has been thoroughly reviewed by Evans [13] and Sheffield [14].

The condition for scattering from the collective electron fluctuations is $(|\vec{k}|\lambda_D)^{-1} \geq 1$ where λ_D is the electron Debye length and $|\vec{k}| = |\vec{k}_o - \vec{k}_s| = (4\pi n_r \sin\theta/2)/\lambda_0$ where $\vec{k}$ is the plasma fluctucation wavevector, $\vec{k}_o$ and $\vec{k}_s$ are the incident and scattered wavevectors, λ_0 is the source wavelength, θ is the scattering angle, and n_r is the refractive index. In tokamak ignition experiments λ_D will be on the order of 50μm, therefore a source wavelength of approximately 0.5mm or longer would be needed for a 90° scattering angle diagnostic. Much shorter wavelength sources can be used at smaller scattering angles, for example, at angles less than 1° 10μm CO^2 lasers have been proposed for alpha particle diagnostics[15]. However, use of long-pulse, millimeter-wave sources offers many advantages in addition to large scattering angles.

1.2 Advantages of Long-Pulse, Millimeter-Wave Scattering

Relative to lasers, a higher signal to noise ratio and a lower diagnostic beam power requirement are an advantage with the use of long-pulse, millimeter-wave sources such as the gyrotron. Signal to noise ratio increases as the square root of integration time. Therefore, the long-pulse/cw capability of a gyrotron, at high-power, can substantially increase this ratio.

The scattered signal is also maximized by using the longest possible diagnostic wavelength. The absolute Doppler broadening and diffraction limited scattering volume vary with wavelength such that the scattered signal in WHz^{-1} scales as λ_0^2. However, much of the signal level increase due to longer wavelength is usually traded off for a larger scattering angle which reduces the scattered signal in WHz^{-1} as $(\sin\theta/2 \sin\theta)^{-1}$. Taking into account the dependence on bandwidth, the signal to noise ratio will scale as $\lambda^{3/2}$ and $(\sin\theta/2)^{-1/2}(\sin\theta)^{-1}$ [16].

With these pulse-length and wavelength scalings it is possible for a gyrotron alpha particle diagnostic to achieve a signal to noise ratio of greater than 1,000 with a 100 kW, 10 ms, millimeter-wave beam in a dense ignited plasma ($n_e \approx 10^{15}cm^{-3}$, $n_\alpha \approx 10^{13}cm^{-3}$) at scattering angles greater than 10°, assuming low background plasma noise. Plasma emission or broadband stray diagnostic beam radiation will reduce the achievable signal to noise ratio. However, the high signal to noise ratio capability gives a gyrotron alpha particle diagnostic significant margin for working. Such a capability is not possible with present high-power pulsed laser technology.

In addition, with a cw gyrotron, the alpha particle parameters could be continuously monitored for the entire length of a tokamak burn pulse. The long pulse capability could also be used to increase the frequency resolution (which also depends on the square root of integration time) for improved alpha particle velocity resolution. A 200 GHz, 90° scattering diagnostic with 100 MHz frequency channels would have an alpha particle velocity resolution $\Delta v/v_\alpha \leq 1\%$ where v_α is the velocity of a 3.5 MeV alpha.

There are other substantial advantages to using millimeter-waves. Millimeter-wave receiver technology is well developed with lower noise temperature and larger bandwidth than available at shorter wavelengths. A single millimeter-wave receiver can have sufficient bandwidth to detect the entire plasma ion velocity distribution spectrum to over the 3.5 MeV alpha birth velocity. In dense plasmas the refractive index for millimeter-wave propagation is generally less than one which helps meet the condition for collective Thomson scattering at all angles. The large scattering angles possible, up to 180°, are an advantage for spatial resolution, stray diagnostic beam rejection, and tokamak access. Finally, millimeter waveguide and antenna components can be relatively radiation tolerant in the environment of an ignition tokamak.

It should also be noted that with the capability to detect the entire plasma ion velocity distribution this diagnostic could provide a localized ion temperature measurement of the bulk plasma in addition to the alpha particle parameters. Plasma instability fluctuation detection could also be another useful by-product of this diagnostic.

2. GYROTRON CAPABILITIES

The gyrotron is currently the best developed source of high-power, long-pulse, millimeter-wave radiation. Its development has been spurred by the need for electron cyclotron heating (ECH) sources for tokamaks; however, its value for plasma diagnostics has also been long recognized [17-20]. Other high-power sources of millimeter-wave radiation such as the cyclotron auto resonance maser (CARM) [21] and free electron laser (FEL) are not as well developed, but may be available in the future for diagnostic applications where higher peak power and higher frequency than possible with a gyrotron are required.

At frequencies of 28, 35, 60, 70, and 140 GHz long pulse/cw gyrotrons are commercially available at power levels up to 200 kW [22]. Recent short pulse experiments relavant to cw operation have demonstrated over 600 kW at 140 GHz and over 400 kW at 243 GHz [23]. Based on the success of these experiments a 1 MW, cw 140 GHz gyrotron is being commercially developed [22]. The identification of ECH as an alternative heating scheme for the 10 Tesla compact ignition tokamak (CIT) will extend this technology to 280 GHz and higher. Therefore, high-power gyrotrons at frequencies needed for collective Thomson scattering alpha particle diagnostics will be readily available.

For plasma diagnostics the quality of the millimeter-wave beam in terms of frequency stability, linewidth, and spatial mode is also important. Recent measurements of a 137 GHz gyrotron developed for plasma diagnostics revealed a linewidth of about 100 kHz FWHM (full width at half maximum) when heterodyned with an unlocked tripled Gunn oscillator and only 100 Hz HWHM when homodyned for a 60 ms pulse [24]. Frequency stability of this gyrotron during the flat top portion of its pulse was well under 1 MHz.

Narrow linewidth and good frequency stability are important to collective Thomson scattering because the linewidth will determine how small a Doppler shift can be observed, and linewidth and frequency stability will determine how effective a frequency notch filter will be in rejecting stray gyrotron radiation. The gyrotron performance in this respect rivals the best molecular laser sources.

Excellent spatial mode and linear beam polarization have also been achieved with gyrotrons using efficient mode convertors. High-power, high frequency gyrotrons generally operate in higher order waveguide modes. This requires mode conversion to launch a linearly polarized beam peaked on axis. Overmoded waveguide convertors have been successfully developed for converting and launching circular TE_{on} gyrotron radiation as a Gaussian beam width efficiencies greater than 90% at frequencies up to 140 GHz [25, 26]. Higher frequency and megawatt gyrotrons will operate in circular $TE_{m,n}$ modes with m>>1. For these modes quasi-optical convertors [27] may be required which have also been demonstrated with good efficiencies at up to 140 GHz [28].

3. SCATTERED SIGNALS

The Thomson scattered signal level in WHz^{-1} is given by

$$P_s=P_o n_e r^2_e L d\Omega \Gamma(\theta,\phi,\chi) S(k,\omega)/2\pi \qquad (1)$$

where P_o is the total incident power in Watts, n_e is the electron density, $r_e=2.8 \times 10^{-13}$cm is the classical electron radius, L is the length of the scattering volume along the source beam, $d\Omega$ is the solid angle of signal collection, $\Gamma(\theta,\phi,\chi)$ is a geometrical form factor, and $S(k,\omega)$ is the spectral density function in per radian units.

For diffraction limited Gaussian optics the product of the scattering length and solid angle of collection can be approximated by

$$L d\Omega \approx \frac{\lambda_o}{F^{\#} \sin\theta}$$

where F# is the receiver optics F number [16].

The geometrical form factor gives the coupling between the incident and scattered beams as it depends on the scattering angle, θ, the polarization angle, ϕ, of the incident electric field relative to the scattering plane (plane containing the incident and scattered beams), and the angle, χ, of the magnetic field B, relative to the scattering plane. For scattering in a plasma with no magnetic field or for ordinary mode (o-mode) scattering in a plasma with a magnetic field, the geometrical form factor using a linearly polarized source is given by

$$\Gamma_o=1-\sin^2\theta\cos^2\phi \qquad (2)$$

In this case it is possible in practice to choose ϕ such that $\Gamma=1$.

For extraordinary mode (x-mode) scattering the geometrical form factor is more complicated. Bretz [20] has derived its form for $\chi=90°$ as

$$\Gamma_x = \frac{\beta(1-b^2-\beta)^2\sin^2\theta+(\gamma-\beta[\beta-1])^2\cos^2\theta}{\gamma^3(1-b^2-\beta)} \qquad (3)$$

where $b=\omega^2_e/\omega^2_o$, $\beta=\Omega^2_e/\omega^2_o$, and $\gamma=1-b-\beta$ where ω_e is the plasma frequency, Ω_e is the electron cyclotron frequency, and ω_o is the diagnostic source frequency. In this case the geometrical form factor is less than one, though not usually by a large factor for typical tokamak diagnostic parameters.

3.1. Spectral Density Function

All the information on the plasma ion velocity distribution and composition is represented by the spectral density function. Its derivation in the non-relativistic and longitudinal approximation limits has been well documented [14] and the results are used here. The form of this function for the fluctuation wavevector $\vec{k} = \vec{k}_s - \vec{k}_o$ and frequency $\omega = \omega_s - \omega_o$ where the subscripts o and s refer to incident and scattered beams is

$$S(k,\omega) = \frac{2\pi}{k} \frac{|1+\sum_i G_i|^2 f_e + |H_e|^2 \sum_i b_i f_i}{|1+H_e+\sum_i G_i|^2} \qquad (4)$$

where the subscripts e and i refer to electrons and the i^{th} ion species, $f_{e,i}$ are the one-dimensional velocity distribution functions along the direction of $\vec{k}$, G_i are the ion screening integrals without a magnetic field, H_e is the screening integral for electrons in a magnetic field, and $b_i = Z_i^2 n_i/n$ where Z_i and n_i are the charge and density of the i^{th} ion and $n = \sum_i n_i Z_i$.

The general form of the screening integrals can be found in Sheffield [14]. For charged particles with non-relativistic, Maxwellian velocity distributions

$$f_{e,i} = \frac{\exp[-(\omega/k_B v_{e,i})^2]}{\pi^{1/2} v_{e,i}}, \quad v_{e,i} = \left(\frac{2k_B T_{e,i}}{m_{e,i}}\right)^{1/2} \qquad (5)$$

where k_B is Boltzman's constant, $T_{e,i}$ is the electron or i^{th} ion species temperature, and $m_{e,i}$ is the particle mass, the screening function for unmagnetized ions is given by

$$G_i = \alpha^2 Z_i \left(\frac{n_i}{n_e}\frac{T_e}{T_i}\right) \left[Rw\left(\frac{\omega}{kv_i}\right) - iIw\left(\frac{\omega}{kv_i}\right)\right] \qquad (6)$$

and that for magnetized electrons by

$$H_e = \alpha^2\left\{1+e^{-k_\perp^2\rho_e^2} \sum_{\ell=-\infty}^{\infty} I_\ell(k_\perp^2\rho_e^2) \left[Rw\left(\frac{\omega-\ell\Omega_e}{k_{||}v_e}\right) - iIw\left(\frac{\omega-\ell\Omega_e}{k_{||}v_e}\right) - 1\right]\right\} \qquad (7)$$

where $\alpha = (k\lambda_D)^{-1}$, Salpeter parameter

$k_\perp = |\vec{k}| \sin\psi$, component of $\vec{k}$ perpendicular to $\vec{B}$

$k_{||} = |\vec{k}| \cos\psi$, component of $\vec{k}$ parallel to $\vec{B}$

ψ, angle of $\vec{k}$ to $\vec{B}$

$\Omega_e = e|B|/m_e$, electron cyclotron frequency

$\rho_e = \frac{v_e}{\sqrt{2}\Omega_e}$, electron gyroradius

$I_\ell(x)$, modified Bessel function of order ℓ

$Rw(x) = 1-2xe^{-x^2}\int_0^x e^{p^2}dp$

$Iw(x) = \sqrt{\pi}\, xe^{-x^2}$

The functions Rw(x) and Iw(x) are related to the plasma dispersion function $Z(x_\ell)$ as $1+x_oZ(x_\ell) = Rw(x_\ell)-iIw(x_\ell)$.

In Eq. 7 only the term for $\ell = 0$ in the summation is significant because Ω_e is generally much larger than the maximum ω being considered here.

The importance of whether to include or not to include the magnetic field in treating the electrons and ions is determined by the size of the charged particles' radius of gyration $\rho_{e,i}$ relative to the fluctuation wavelength $2\pi/k$ being studied. For plasma conditons typical in tokamaks $k\rho_e<<1<<k\rho_i$ is generally true. The electron gyration radius is small compared to the resolved fluctuation wavelength. Therefore the scattered spectrum will be affected by the restriction on the electron motion across the magnetic field for orientation of $\vec{k}$ to $\vec{B}$ near 90°. On the other hand, the gyration radius of the ions including the alpha particles is large relative to the resolved fluctuation wavelength. Therefore, as originally shown by Salpeter [30] and Renau [31], the ion screening integrals can be approximated by their unmagnetized form.

It is not strictly correct to ignore the magnetic field for the ions. Hagfors [32] has shown that by including the effect of the magnetic field for $k\rho_i>>1$ the scattered spectrum will be modulated at approximately the ion cyclotron frequency for a very restricted orientation of $\vec{k}$ to $\vec{B}$ near 90°. However, in practice, this modulation will probably not be observable because of finite frequency resolution. Consequently the detected spectrum envelope is essentially that for unmagnetized ions.

3.1.1 Calculations without Magnetic Field

The spectral density function (Eq. 4) was evaluated as a function of frequency for several different assumed alpha particle velocity distributions and fractional densities in a D-T plasma as shown in Figs. 1 and 2. The orientation of $\vec{k}$ to $\vec{B}$ was chosen to be sufficiently far away from perpendicular ($\psi<80°$) to avoid

magnetic field effects. These frequency spectrums correspond to what would be detected by a receiver and clearly demonstrate the effectiveness of this diagnostic for alpha particle velocity distributution and density measurements. The 200 GHz scattering frequency and high density plasma conditions are representative of the CIT.

Three different one-dimensional alpha particle distribution functions were considered in Fig. 1: a hot Maxwellian as given by Eq. 5 with T_α = 500 keV, a constant velocity distribution given by

$$f_\alpha = \frac{1}{2v_\alpha}, \quad |\vec{v}| \le v_\alpha$$
$$f = 0, \quad |\vec{v}| > v_\alpha \tag{8}$$

and a beam slowing-down distribution [33] given by

$$f_\alpha = \frac{C_o v^2}{v^3+v_c^3}, \quad |\vec{v}| \le v_\alpha$$
$$f = 0, \quad |\vec{v}| > v_\alpha \tag{9}$$

where

$$C_o = \frac{3}{2\ell n\left(1+\left(\frac{v}{v_c}\right)^3\right)}$$

$$v_c = \left(\frac{3\sqrt{\pi m_e Z_i}}{4M_\alpha}\right)^{1/3} v_e$$

$$Z_i = \sum_i \frac{n_i Z_i^2}{n_e M_i} M_\alpha$$

For these distribution functions $v_\alpha = 1.3 \times 10^7$m/sec, the alpha birth velocity, and it was assumed that there is no upward scattering in velocity space, therefore the distribution functions and corresponding spectrums are sharply terminated at this velocity. Also, it was assumed that $G_\alpha = 0$ for the non-Maxwellian distributions. This is exactly true for the constant velocity distribution because the screening function is proportional to df_α/dv and justified for the slowing down distribution because G_α is very small relative to the other G_i's in the summations of Eq. 4.

It is presently thought that the slowing-down distribution is the most likely to occur. In Fig. 2 the dependence of the spectrum on the fraction of alphas with this distribution is shown. A relative measure of the large Doppler shifted alpha signal to the small Doppler shifted bulk ion signal can provide a sensitive measure of the fraction of alpha particles in the plasma. This would be possible without the need for absolute signal level calibration.

3.1.2 Calculations with Magnetic Field

The direction of the magnetic field relative to $\vec{k}$ effects the scattered spectrum when the angle of $\vec{B}$ to $\vec{k}$ is near 90°. This is illustrated in Fig. 3 where Eq. 4 is plotted for three angles of $\vec{B}$ to $\vec{k}$ between 90° and 87°. For angles less than 80° the spectrum is essentially the same as given in Figs. 1 and 2. The sharp resonance which occurs in the alpha feature of the spectrum was noted by Vahala et al [34] and was identified with the lower hybrid resonance which in a cold plasma has a dispersion relation given by

$$\omega^2 = \frac{\omega_i^2}{1+\omega_e^2/\Omega_e^2}\left(1+\frac{m_i}{m_e}\frac{k_\parallel^2}{k_\perp^2}\right) \qquad (10)$$

where ω_e and ω_i are the electron and ion plasma frequencies. This resonance is much sharper here than in Ref. 34 because the magnetized electron screening function is used in the numerator of Eq. 4.

On first inspection it would seem that this resonance, which increases the scattered signal level by several orders of magnitude at its peak, could greatly improve the prospects for detection of alpha particles in an ignition tokamak experiment. However, because of the sharpness of this resonance and its critical dependence on the orientation of $\vec{B}$ to $\vec{k}$, the divergence of the diagnostic source beam and receiver field of view will largely "wash-out" this resonance. This is demonstrated in Fig. 4 by integrating the spectral density function over realistic millimeter-wave beam divergences.

The beam divergence integration was carried out only in one dimension along the direction of ψ variation and weighted by a Gaussian beam profile,

$$S_\psi(k,\omega) = \sqrt{\frac{2}{\pi}}\frac{1}{\Delta\psi}\int_{-\sqrt{\pi}\Delta\psi}^{\sqrt{\pi}\Delta\psi} e^{-2\left(\frac{\psi-\psi_o}{\Delta\psi}\right)} S(k,\omega)d\psi \qquad (11)$$

where $\Delta\psi = \sqrt{2}\lambda_o/0.6435\pi a$ is the convolved $1/e^2$ divergence angle of equal source and receiver beams with antennae aperture radii a. A two dimensional integration which would take into account the spread in scattering angle, θ, would not significantly alter the results of Fig. 4 because the spectral density function is not sensitive to a small divergence in a large scattering angle.

For the calculations of Fig. 4 source and receiver beam antenna apertures of 5 cm diameter were assumed which at 200 GHz would correspond to Gaussian divergences of 1.2° full width at half maximum (FWHM). An orientation angle of $\vec{B}$ to $\vec{k}$ slightly less than 90°, $\psi_o = 88°$ seems to enhance the alpha component of the scattered spectrum the most. Except for a peak corresponding to the resonance frequency for $\psi = 90°$, the alpha component is increased by a factor of 2 to 3 and is distorted relative to the unmagnetized spectrum. However, the dependence on the alpha particle velocity distribution is still very clear as shown by the two curves.

It may be possible to use this lower hybrid resonance in the scattered spectrum to diagnose the direction of the local magnetic field. Previous magnetic field direction measurements by thermal level collective Thomson scattering used the frequency narrowing of the bulk ion feature [10]. The accuracy of such a measurement could be significantly improved by using a resonance peak in the scattered spectrum as originally suggested by Siegrist et al [35].

4. SIGNAL TO NOISE RATIO

The dependence of the collective Thomson scattered signal on the fusion alpha particle parameters demonstrates that this will be a good alpha particle diagnostic. However, to assess its potential for working, the achievable signal to noise ratio has to be considered.

The scattered signals are noise-like, broadband fluctuating levels due to the thermal nature of the plasma fluctuations. Competing background signals, due to plasma emission or the receiver noise temperature, are also generally incoherent, broadband fluctuating levels. In this case the signal to noise ratio is defined as the ratio of the scattered signal level to the root mean square (rms) uncertainty in the combined scattered and background signals given by [36]

$$S = \frac{P_s}{P_s + P_N}\sqrt{1 + \Delta f \tau} \qquad (12)$$

where P_s is the scattered signal given by Eq. 1, P_N is the background signal, Δf is the bandwidth of a receiver channel, and τ is the integration time.

According to Eq. 12 it is important to have a large time-bandwidth product, $\Delta f \tau$, in order to have large signal to noise ratio. The bandwidth is limited by the parameters of the experiment and the desired frequency resolution. Therefore, a long integration time is necessary for achieving a high signal to noise ratio. In this respect long pulse cw gyrotron sources have a distinct advantage over high-power lasers which are generally limited to microsecond pulses. For example, a resolution bandwidth of about 1 GHz would be needed to resolve the various alpha particle velocity distributions shown in Fig. 1. Combined with a 10 ms gyrotron pulse this would correspond to a maximum possible signal to noise ratio of $\sqrt{\Delta f \tau}$ = 3,160. In contrast, previous laser scattering diagnostics [9-12] to measure the bulk ion thermal feature where Δf was limited to about 100 MHz and τ to about 1 μs had maximum possible signal to noise ratios of $\sqrt{\Delta f \tau} \approx 10$. The large improvement in achievable signal to noise ratio gives a gyrotron alpha particle diagnostic significant margin for working.

Diagnostic integration time would not have to be limited just to 10 ms with a gyrotron. Much longer integration times would be possible to detect very weak signals in a strong background. In such a case the gyrotron beam may need to be modulated and synchronous signal detection used to fully realize the signal to noise ratio given by Eq. 12.

A sample signal to noise ratio calculation for a CIT gyrotron alpha particle diagnostic is given in Table 1. It was assumed that 100 kW diagnostic beam power

was incident at the plasma and that the spectral density corresponds to a 0.5% fraction of alphas if not enhanced by magnetic field orientation (see Fig. 2) or a smaller fraction if an optimum magnetic field orientation is used. Furthermore, since the scattered spectrum should be broadened symmetrically up and down in frequency, it was assumed that double sideband (DSB) detection is used.

The spectrum could be asymmetric if there is a plasma current. However, in order for the asymmetry to be significant the electron drift velocity $\vec{v}_D$, would need to be a large fraction of the thermal velocity and the orientation of $\vec{k}$ would need to have a large component along $\vec{v}_D$. It is possible to chose a scattering geometry in the poloidal plane of a tokamak where asymmetry in the scattered spectrum is unlikely. In such a case, x-mode scattering perpendicular to the magnetic field would reduce the scattering cross section by the geometrical form factor as evaluated by Eq. 3 and given in Table I for CIT. The resulting signal to noise ratio of over 200 is possible with 10 ms integration if the background signal, P_N, is limited to a receiving system noise temperature of approximately 10,000K DSB.

It is the assumption on the background signal level which is the most optimistic in this calculation. Plasma emission at millimeter-wave frequencies and scattering from waves and instabilities could significantly exceed the receiver temperature. However, it should be noted that only wideband, incoherent sources of background need to be included in P_N of Eq. 12. A narrow band source could be rejected with a filter and a coherent source could be cancelled out by an interferometric technique. For example, strong stray narrowband radiation from the source would be rejected by a notch filter and would not enter into the calculation of signal to noise ratio.

A wideband, incoherent signal background a factor of 10 higher than assumed in Table I would still leave this diagnostic with a useful signal to noise ratio of over 20. Higher backgrounds could be compensated for by longer integration time and/or higher diagnostic beam power. The optimization of the diagnostic source parameters for high backgrounds can best be visualized by recasting Eq. 12 in terms of source energy, $\varepsilon_o = P_o\tau$,

$$S = \frac{\sqrt{\Delta f \varepsilon_o P_o}}{P_o + P_N/\xi} \quad \text{for } \Delta f\tau >> 1 \qquad (13)$$

where ξ is defined by $P_s = \xi P_o$ and Eq. 1. The importance of long integration time is now translated to the importance of high energy capability of the diagnostic beam source. The signal to noise ratio increases as the square root of energy, just as it does with integration time.

The most effective way to overcome high backgrounds is to increase the diagnostic beam energy through an increase in peak power. As pointed out in Section 2, megawatt cw gyrotrons are under development and should be considered for use in plasmas where a large emission background is expected. It is also possible to compensate for high backgrounds by just increasing source energy through a longer pulse length. Present 100 kW gyrotron capability with

pulse lengths of up to one second should be useful for diagnostics with background P_N's of up to 10^{-16} WHz^{-1} in dense plasmas (~$10^{15}cm^{-3}$) with large alpha fractions (~2%).

It is also possible to partially compensate for high backgrounds by just increasing peak power (through a reduced pulse length) when $P_s < P_N$. This would not be a complete substitute for higher diagnostic beam energy. Fig. 5 illustrates this where signal to noise ratio is plotted as a function of source peak power for the parameters given in Table I, except for pulse length which is allowed to vary to keep energy constant. There is an optimum diagnostic peak power which increases with background level. However, increasing the source peak power to this optimum does not fully recover the signal to noise ratio without increasing source energy also.

5. ACCESSIBILITY OF MILLIMETER-WAVES TO TOKAMAK PLASMAS

In dense (>$10^{13}cm^{-3}$), high field (>1 Tesla) plasmas typical of tokamaks a number of resonances and cutoffs occur in the millimeter-wavelength range of the electromagnetic spectrum. These resonances and cutoffs must be avoided for a successful scattering diagnostic. The electron cyclotron resonance and its harmonics are of particular concern because they will be strong sources of background emission and absorption. The harmonics above the 2nd will be overlapped in frequency because of the spatial dependence of the tokamak magnetic field and because of relativistic frequency broadening at the high electron temperatures (>10 keV) expected in an ignition experiment. A scattering diagnostic must therefore use a frequency which is above the highest significant electron cyclotron harmonic or be below the fundamental (1st harmonic). It may also be possible in some cases to go between the 1st and 2nd harmonics.

Using frequencies sufficiently high to get above the highest significant harmonic would rule out millimeter- and submillimeter-wave diagnostics in high-field tokamaks. For example, in the 10 Tesla CIT experiment the electron cyclotron resonance would be at 280 GHz at the plasma center. If a 25 keV electron temperature is reached, the 10th harmonic would have an optical depth of approximately 0.06 for extraordinary mode propagation perpendicular to the magnetic field [37]. Even if the scattering geometry avoids x-mode propagation there would still be a source of 1.5 keV equivalent black body emission (2.4 x $10^{-16}WHz^{-1}$) in the tokamak for which very effective viewing dumps would be needed. However, submillimeter-wave beam dump technology is not well developed for much more than 10dB rejection [38,39]. This would seem to rule out the 1 to 0.1mm wavelength range for this diagnostic in an ignition tokamak such as CIT. Use of laser sources with wavelengths of 100μm and shorter would limit this diagnostic to scattering angles less than 10° and would not have the other advantages of long-pulse millimeter-wave scattering.

At frequencies below the fundamental electron cyclotron resonance millimeter-waves can be used for diagnostics. In fact it appears that millimeter-wave accessibility below the electron cyclotron resonance is a natural consequence of high-field tokamak operation. The lower limit to a diagnostic frequency is an electron density dependent cutoff. For o-mode propagation this is just the electron

plasma frequency $\omega_e(\approx 8.97\sqrt{n_e[m^{-3}]}\,Hz)$. For x-mode it is the electron plasma frequency as lowered by the magnetic field

$$\omega_{1,(2)} = [(\Omega_e/2)^2 + \omega_e^2] - (+)\,\Omega_e/2 \qquad (14)$$

where ω_1 is the lower x-mode cutoff frequency of interest here and ω_2 is the upper x-mode cutoff frequency above Ω_e. It has been found experimentally by Murakami et al [40] that the maximum plasma density in a tokamak scales as

$$n_e \propto \frac{B}{R}$$

where B and R are the tokamak field and major radius, respectively. As the magnetic field of a tokamak is increased the cutoff frequencies will increase at most as the square root of field while the electron cyclotron resonance will increase linearly with field. A gap in frequency space between the density cutoff limits and the electron cyclotron resonance, which is largest for x-mode propagation, will therefore exist for diagnostics provided the field is high enough and the tokamak is not too compact.

These resonances and cutoffs between which a diagnostic frequency must be found are illustrated in Fig. 6. Frequency normalized to the central magnetic field is plotted as a function of normalized major radius. The first four electron cyclotron harmonics are plotted as well as the lower x-mode cutoffs for three tokamaks that are expected to produce alpha particles. Parabolic density profiles were assumed with peak densities of $1 \times 10^{14} cm^{-3}$ for TFTR and JET, and $6 \times 10^{14} cm^{-3}$ for CIT. The resulting diagnostic frequency windows between the peak x-mode cutoff frequency at the plasma center and the minimum electron cyclotron resonance on the outside edge of the tokamak are: 55-67 GHz JET, 43-109 GHz TFTR, and 122-213 GHz CIT assuming central fields of 3.4, 5.2, and 10 Tesla, respectively.

In reality, these millimeter-wave diagnostic windows based on a cold temperature plasma model are not so well defined. Hot electron effects such as Cerenkov emission if runaway electrons are present [41], and relativistic down shifting of the electron cyclotron resonance can significantly constrain these windows. Of primary concern is relativistic down shifting of the electron cyclotron resonance. At an electron temperature of 25 keV the optical depth of o- and x-mode propagation perpendicular to the magnetic field at half the cold electron cyclotron frequency would be comparable to that for x-mode at the 10^{th} harmonic [37]. This would constrain the upper frequency limit of the diagnostic window to be as low as possible relative to the electron cyclotron resonance at the plasma center. X-mode propagation in this case provides an advantage in displacing the electron cyclotron resonance upward in frequency to the upper hybrid resonance

$$\omega_u = (\omega_e^2 + \Omega_e^2)^{1/2} \qquad (15)$$

as shown in Fig. 6.

The JET millimeter-wave window is the most marginal because of that tokamak's low magnetic field. Even using a frequency between the 1st and 2nd harmonics in o-mode to avoid the upper x-mode cutoff (not shown in Fig. 6) would be marginal because JET's low aspect ratio causes these harmonics to overlap. However, a scattering geometry that accesses the plasma as close to vertical as possible may make feasible the use of 70 GHz x-mode or 140 GHz o-mode for this diagnostic. It should also be possible in JET to get above the highest significant electron cyclotron harmonic in the submillimeter wavelength range if a suitable source were available in the 400 to 100μm range.

In TFTR and CIT the millimeter-wave diagnostic windows appear large enough to be usable, particularly in TFTR where a commercially available 60 GHz gyrotron could be used more than a factor of two below the central electron cyclotron resonance. Even a frequency between the 1st and 2nd cyclotron harmonics would be more feasible in these tokamaks because their larger aspect ratios avoid a spatial frequency overlap between these harmonics.

Additional issues which must be assessed in determining the accessibility of millimeter-waves for diagnostics in tokamaks are Faraday rotation and plasma turbulence. Boyd [41] has shown that when the anisotropy between o- and x-mode indices of refraction is large, as in a tokamak for electron cyclotron harmonics below the fifth, then the polarization of the propagating radiation is locally preserved and Faraday rotation does not occur. Plasma turbulence is a well documented phenomena in tokamaks [42] and there can be very high relative fluctuation levels $\tilde{n}/n$ approaching 100% at the plasma edge. However, the absolute fluctuating densities are low and the resulting attenuation on a scattering diagnostic would be minimal. The main effect would be to increase the level of stray background radiation which could be filtered.

6. REFRACTION AND RAY TRACING

Refraction deserves special consideration. The refractive index in a plasma can deviate from one when the propagating frequency is near a resonance or a cutoff. Furthermore, since tokamak plasma resonances and cutoffs are functions of position, extended refractive index gradients will be present. Such gradients can bend, diverge, and/or focus a propagating beam. The severity of these effects need to be considered to further refine the frequency limits of millimeter-wave accessibility for diagnostics in tokamaks.

It is possible under some conditions to choose a scattering geometry that minimizes the effect of refraction. A ray propagating parallel to the refractive index gradient will not be deflected. Also, the larger the scattering angle the less sensitive the scattered spectrum will be to small angular deviations. For example, a large angle scattering diagnostic localized at the center of a circularly symmetric plasma would not have its average scattering angle, location, or spectrum changed by refraction. In practice, however, D-T burning tokamaks will not have circulary symmetric plasmas and off center profile information will be required of any practical alpha particle diagnostic.

The general effect of refraction for high diagnostic frequencies $\omega_0 > \Omega_e$ will be to defocus and deflect the diagnostic beam from the center of the plasma because the refractive index is less than one and decreasing with increasing

density. However, for the proposed x-mode diagnostic window at frequencies below Ω_e the refractive index can be greater than one when $\omega_e < \omega_o < \Omega_e$ [43]. In this case the diagnostic beams could be focused toward the plasma center. At higher peak plasma densities, $\omega_e > \omega_o$, an x-mode ray propagating into the plasma could be alternately bent toward and away from the plasma center. This would be an advantage for x-mode propagation because the ω_1 cutoff could be approached closer than the ω_e o-mode cutoff.

Ray tracing calculations were carried out for possible scattering geometries in the poloidal plane of representative tokamaks. The ray equation [44],

$$\frac{1}{\rho} = \frac{\text{grad } n_r}{n_r} \sin \phi \qquad (16)$$

was numerically solved on a computer, where ρ is the radius of ray curvature, n_r is the refractive index, and ϕ is the angle between the ray and grad n_r. The refractive index for x-mode propagation in a cold plasma [44],

$$n_r = \left[\frac{(\omega_o^2-\omega_1^2)(\omega_o^2-\omega_2^2)}{\omega_o^2(\omega_o^2-\omega_u^2)}\right]^{1/2} \qquad (17)$$

was used, where ω_1 and ω_2 are given by Eq. 14 and ω_u by Eq. 15. Eq. 17 would correspond to o-mode propagation if the magnetic field were reduced to zero. Two electron density profiles were considered, a parabolic one

$$n_e = n_o\left[1-\left(\frac{r}{r_o}\right)^2\right] \qquad (18)$$

and a much steeper sinc^2 one

$$n_e = n_o\left[\frac{\sin(\pi\frac{r}{r_o})}{\pi\frac{r}{r_o}}\right]^2 \qquad (19)$$

where

$$\frac{r}{r_o} = \frac{x+\Delta x}{a} + \frac{y}{b} \qquad (20)$$

x,y are the cartesian coordinates relative to the plasma center

a is the horizontal minor radius

b = Ea where E is the vertical elongation

$$\Delta x = \delta a\left[1-\sqrt{1-\left(\frac{y}{b}\right)^2}\ \right] \quad \text{where } \delta \text{ is the shape factor.}$$

Eq. 20 is a good approximation of the D-shaped plasmas being planned for ignition experiments. A $sinc^2$ density profile was considered because recent results such as the TFTR supershots [45] show that very steep density profiles may be possible in ignition experiments. The $sinc^2$ profile approximates a Gaussian with the nice property of going to zero at the edges.

This is a very simple ray tracing model. A more accurate model would need to include warm plasma effects and actual density profiles and plasma shapes. An extension to three dimensions should also be made. However, for purposes here this model is sufficient to assess the severity of refractive effects on a millimeter-wave scattering diagnostic.

Calculations representative of a possible CIT diagnostic are shown in Fig. 7 and 8. The CIT parameters at the time of this writing are: major radius 1.75m, minor radius 0.55m, a 10 Tesla field capability, and achievable elongation and shape factors as shown. The maximum density expected is between 5 and 6 x $10^{14}cm^{-3}$. Three pairs of parallel rays seperated by 6cm are shown entering the plasma. Two of the pairs are directed horizontally from the outside of the tokamak and one pair from the top to the bottom toward the center. The gyrotron and receiver field of view could be represented by any pair of orthogonal beams for a 90° scattering angle. Diffraction effects need not be considered to first order because the collimation (Rayleigh) range of a 200 GHz Gaussian beam with a $1/e^2$ diameter of 6cm is about 2m, the maximum path length through CIT.

Fig. 7 shows that x-mode refraction is not a severe effect at 200 GHz for the maximum predicted densities in CIT. Even with the steep $sinc^2$ density profile the diagnostic beams are fairly well defined and directed. The horizontal beam directed at the center of the plasma with a $sinc^2$ profile is actually focused, which would be beneficial to a scattering diagnostic.

The x-mode cutoff density at 200 GHz and 10 Tesla is 1.2 x $10^{15}cm^{-3}$. The results of Fig. 7 demonstrate that for peak densities to within half this value refraction is not detrimental to diagnostics. If the peak density is increased to within 20% of the cutoff value, as shown in Fig. 8, then refraction is much more significant, though diagnostics may still be possible. The off center and vertical beams are effected most because they cut across refractive index gradients. With the parabolic density profile the data would need to be corrected for changes in spatial resolution, position, and scattering angle. With the $sinc^2$ profile the vertical beam is deflected completely away from the plasma center. It may be possible in this case to change the beam launch direction to partially compensate for refraction.

A practical lower frequency limit for x-mode diagnostics would therefore probably be for ω_1 evaluated at a density about 20% higher than expected. This would correspond to 50, 62, and 140 GHz in TFTR, JET, and CIT, respectively, for the densities and fields given in Section 5.

7. SUMMARY

There is an important need for alpha particle fusion product diagnostics in D-T burning tokamaks. Collective Thomson scattering from ion thermal fluctuations is potentially a powerful diagnostic technique for satisfying this need. Its attributes include an unperturbing, space and time localized measure of the alpha particle velocity distribution and density. This is accomplished in a direct and unambiguous way by detecting a scattered spectrum which is Doppler broadnened by the ion velocities. Only for a restricted orientation of the scattering plane near perpendicular to the magnetic field will the scattered spectrum be complicated by magnetized particle effects. Even in this orientation the magnetic effects will be largely "washed out" by finite diagnostic beam divergence and limited frequency resolution.

The general criteria for choosing the optimum source for collective Thomson scattering diagnostics are: 1) use the longest wavelength source consistent with the desired diffraction limited spatial resolution and plasma accessibility, and 2) use the longest pulse source with sufficient peak power consistent with the desired temporal resolution and signal to noise ratio. The first criteria arises because the Doppler broadened signal in WHz^{-1} increases with wavelength and/or the scattering angle can be increased for practical implimentation of this diagnostic. The second criteria is due to the scaling of signal to noise ratio with the square root of time. It also implies the need for a high average power source.

The millimeter-wave gyrotron therefore is the best source developed to date for collective Thomson scattering. Its wavelength allows large scattering angles up to 180° with sufficient diffraction limited spatial resolution in large tokamak devices. Its long pulse capabilty at high-power makes possible high signal to noise ratios not previously possible with microsecond lasers. There may be good millimeter-wave diagnostics accessibility in tokamak plasmas for x-mode propagation between the lower x-mode cutoff and the upper hybrid resonance. In addition, millimeter-wave receiver technology is well developed with wide enough bandwidth capability to detect the entire alpha particle velocity distribution to over the 3.5MeV birth energy. Millimeter-wave guide techniques may also be more robust than infrared optics in an ignition tokamak radiation environment. All these reasons give a collective Thomson scattering diagnostic based on a long-pulse, millimeter-wave source such as a gyrotron significant potential for working.

ACKNOWLEDEMENTS

The author wishes to acknowledge for many useful and stimulating discussions on this topic N. Bretz, D. R. Cohn, A. E. Costley, P. Efthimion, T. P. Hughes, D. P. Hutchinson, I. H. Hutchinson, J. S. Machuzak, R. C. Myer, R. K. Richards, D. J. Sigmar, R. J. Temkin, G. Vahala, and K. M. Young.

References

1. K. M. Young, Presentations from the workshop on alpha-particle diagnostics on CIT, Princeton University Plasma Physics Laboratory, AA-870710-PPL-06, 3-5 June 1987,

2. O. N. Jarvis & A. E. Costley, A summary of the workshop on alpha-particle diagnostics held at JET on 9-10 December 1986, JET Joint Undertaking, JET-P(87)05.

3. D. Post, S. Zweben, and L. Grisham, Alpha particle diagnostics, 1986 Varenna Diagnostics School.

4. S. J. Zweben, Approaches to the diagnostics of alpha particles in tokamaks, Rev. Sci. Instrum., vol. 57, pp. 1723-1728, 1986.

5. K. L. Bowles, Observation of vertical incidence scatter from the ionosphere at 41Mc/sec, Phys. Rev. Lett., vol. 1, pp. 454-455, 1958.

6. J. V. Evans, Theory and practice of ionosphere study by Thomson scatter radar, Proc. of the IEEE, vol. 57, pp. 496-530, 1969.

7. A. W. DeSilva, D. E. Evans, and M. J. Forrest, Observation of Thomson and co-operative scattering of ruby laser light by a plasma, Nature, vol. 203, pp. 1321-1322, Sept. 26, 1964.

8. S. A. Ramsden and W. E. R. Davies, Observation of co-operative effects is the scattering of a laser beam from a plasma, Phys. Rev. Let., vol. 16, pp. 303-306, 1966.

9. W. A. Peebles and M. J. Herbst, CO_2 laser Thomson scattering from a pulsed hydrogen arc, IEEE Trans. Plasma Sci., vol. PS-6, pp. 564-567, 1978.

10. W. Kasparek and E. Holzhauer, Simultaneous measurement of magnetic field direction and ion temperature in a plasma by collective scattering with a CO_2 laser, Appl. Phys. Lett., vol. 43, pp. 637-638, 1983.

11. P. Woskoboinikow, W. J. Mulligan, J. Machuzak, D. R. Cohn, R. J. Temkin, T. C. L. G. Sollner, and B. Lax, "385mm D_20 laser collective Thomson scattering ion temperature dignostic," Europhysics Conference Abstracts 11th European Conference on Controlled Fusion and Plasma Physics, Aachen, 5-9 September, 1983, Vol. 7D, Part II, pp. 81-84.

12. R. Behn, S. Kjelberg, P. A. King, A. Salito, and M. R. Siegrist, Observation of collective Thomson scattering of D_20 laser radiation from a tokamak plasma, Conference Digest 10th International Conference on Infrared and Millimeter Waves, Lake Buena Vista, Florida, 9-13 December, 1985, IEEE cat. no. 85Ch2204-6, pp. 143-144.

13. D. E. Evans and J. Katzenstein, Laser light scattering in laboratory plasmas, Rep. Prog. Phys., vol. 32, pp. 207-271, 1969.

14. J. Sheffield, Plasma Scattering of Electromagnetic Radiation, New York, Academic Press, 1975.

15. D. P. Hutchinson, K. L. Vander Sluis, J. Sheffield, and D. J. Sigmar, Feasibility of alpha-particle measurement by CO_2 laser Thomson scattering, Rev. Sci. Instrum., vol. 56, pp. 1075-1077, 1985.

16. P. Woskoboinikow, D. R. Cohn, and R. J. Temkin, Application of advanced millimeter/far-infrared sources to collective Thomson scattering plasma diagnostics, Int. J. Infrared and Millimeter Waves, vol. 4, pp. 205-229, 1983.

17. R. J. Temkin, S. M. Wolfe, and B. Lax, Application of high frequency gyrotrons to tokamak heating, Bull. Amer. Phys. Soc., vol. 22, p. 1164, 1977.

18. L. Bighel and T. L. White, Collective scattering of gyrotron radiation for T; measurements on EBT, Oak Ridge National Lab., ORNL/TM-7574, 35 pages, 1981.

19. G. F. Brand, N. G. Douglas, M. Gross, J. Y. L. Ma, L. C. Robinson, and C. Zhizi, A 125-260 GHz gyrotron, IEEE Trans. Microwave Theory and Techniques, vol. MIT-31, pp. 58-64, 1984.

20. P. Woskoboinikow, Development of gyrotrons for plasma diagnostics, Rev. Sci. Instrum., vol. 57, pp. 2113-2118, 1986.

21. V. L. Bratman, N. S. Ginzburg, G. S. Nusinovich, M. I. Petelin, and P. S. Strelkov, Relativistic gyrotrons and cyclotron autoresonance masers, Int. J. Electronics, vol. 51, pp. 541-567, 1981.

22. K. Felch, R. Bier, L. J. Craig, H. Huey, L. Ives, H. Jory, N. Lopez, and S. Spang, Achievements in CW operation of 140 GHz gyrotrons, Conf. Digest 11th Int. Conf. Infrared and Millimeter Waves, Tirrenia, Pisa, Italy, 20-24 October, 1986, pp. 43-45.

23. K. E. Kreischer and R. J. Temkin, Single-mode operation of a high-power, step-tunable gyrotron, Phys. Rev. Lett., vol. 59, pp. 547-550, 1987.

24. P. Woskoboinikow, D. R. Cohn, J. S. Machuzak, and R. J. Temkin, Application of millimeter-wave scattering to diagnostics of fusion alphas, MIT Plasma Fusion Center, PFC/CP-86-16, 28 pages, 1986.

25. J. Trulsen, P. Woskoboinikow, and R. J. Temkin, Circular waveguide mode convertors at 140 GHz, MIT Plasma Fusion Center, PFC/RR-86-2, 58 pages, 1986.

26. M. Thumm, V. Erckmann, W. Kasparek, H. Kumric, G. A. Muller, P. G. Schuller, and R. Wilhelm, Very high power mm-wave components in oversized waveguides, Microwave Journal, vol. 29, pp. 103-121, Nov. 1986.

27. S. N. Vlasov and I. M. Orlova, Quasioptical transformer which transforms the waves in a waveguide having circular cross section into a highly directional wave beam, Radiophysics Quantum Electron., vol. 17, pp. 115-119, 1974.

28. B. G. Danly, K. E. Kreischer, W. J. Mulligan, and R. J. Temkin, Whispering-gallery-mode gyrotron operation with a quasi-optical antenna, IEEE Trans. on Plasma Science, vol. PS-13, pp. 383-388, 1985.

29. N. Bretz, Geometrical effects in x-mode scattering, Princeton Plasma Physics Lab., PPPL-2396, 15 pages, 1986.

30. E. E. Salpeter, Plasma density fluctuation in a magnetic field, Physical Rev., vol. 122, pp. 1663-1674, 1961.

31. J. Renau, H. Camnitz, and W. Flood, The spectrum and total intensity of electromagnetic waves scattered from an ionized gas in thermal equilibrium in the presence of a static quasi-uniform magnetic field, J. Geophysical Research, vol. 66, pp. 2703-2732, 1961.

32. T. Hagfors, Density fluctuation in a plasma in a magnetic field, with applications to the ionosphere, J. Geophysical Research, vol. 66, pp. 1699-1712, 1961.

33. J. D. Gaffey, Jr., Energetic ion distribution resulting from neutral beam injection in tokamaks, J. Plasma Physics, vol. 16, part 2, pp. 149-169, 1976.

34. L. Vahala, G. Vahala, and D. J. Sigmar, Effects of alpha particles on the scattering function in CO_2 laser scattering, Nuclear Fusion, vol. 26, pp. 51-60.

35. M. R. Siegrist, M. A. Dupertuis, R. Behn, and P. D. Morgan, Simulation of a magnetic field and ion temperature measurement in a tokamak by Thomson scattering, Plasma Physics, vol. 24, pp. 1449-1463, 1982.

36. H. Z. Cummins and H. L. Swinney, Light beating spectroscopy, Progress in Optics, vol. 8, pp. 135-200, 1970.

37. B. A. Trubnikov, Magnetic Emission of High Temperature Plasma, Dissertation, Appendix III, Moscow, 1958, USAEC Tech. Information Service AEC-tr-4073, 1960.

38. P. Woskoboinikow, R. Erickson, and W. J. Mulligan, Submillimeter-wave dumps for fusion plasma diagnostics, International J. Infrared and Millimeter Waves, vol. 4, pp. 1045-1059, 1983.

39. K. Kato and I. H. Hutchinson, Nonthermal electron velocity distribution measured by electron cyclotron emission in alcator C tokamak, Phys. Rev. Lett., vol. 56, pp. 340-343, 1986.

40. M. Murakami, J. D. Collen, and L. A. Berry, Some observations on maximum densities in tokamak experiments, Nuclear Fusion, vol. 16, pp. 347-348, 1976.

41. D. A. Boyd, What is the limiting polarization of electron cyclotron emission leaving a fusion plasma, 5th International Workshop on Electron Cyclotron Emission and Electron Cyclotron Heating, EC-5, San Diego, pp. 77-87, Nov. 1985.

42. P. C. Liewer, Measurements of microturbulence in tokamaks and comparisons with theories of turbulence and anomalous transport, Nuclear Fusion, vol. 25, pp. 543-621, 1985.

43. M. A. Heald and C. B. Wharton, Plasma Diagnostics with Microwaves, chap. 1, Robert E. Krieger Publishing Co., Huntington, New York, 1978.

44. M. Born and E. Wolf, Principles of Optics, Sec. 3.2.1., Pergamon Press, Oxford, 5th Edition, 1975.

45. J. D. Strachan, et al, High Temperature Plasmas in the Tokamak Fusion Test Reactor, Phys. Rev. Lett., vol. 58, pp. 1004-1007, 1987.

TABLE I

SIGNAL TO NOISE RATIO CALCULATION FOR 200 GHZ, 90° X-MODE SCATTERING FROM ALPHAS IN CIT.

P_o	100kW
n_e	$6 \times 10^{14} cm^{-3}$
$Ld\Omega$	$10^{-2} sr\ cm$
$S(k,\omega)\frac{d\omega}{2\pi}$	$2 \times 10^{-13} Hz^{-1}$
$\Gamma(\theta,\phi,\psi)$	0.4
P_s	$3.82 \times 10^{-21} WHz^{-1}$ SSB $7.63 \times 10^{-21} WHz^{-1}$ DSB
P_N	$10^{-19} WHz^{-1}$
Δf	1 GHz
τ	10ms
S	224

Figure Captions

1. Collective Thomson scattered ion thermal spectrums as affected by the presence of alpha particles and their velocity distribution.

2. Collective Thomson scattered ion thermal spectrums with different fractions of alpha particles having a slowing down velocity distribution.

3. Collective Thomson scattered ion thermal spectrums for orientation of $\vec{k}$ to $\vec{B}$ near perpendicular. Such spectrums would not be observed in practice because of finite $\vec{k}$ and frequency resolution.

4. Collective Thomson scattered ion thermal spectrums for a $\vec{k}$ to $\vec{B}$ angle of 88°. Spectrums are integrated over realistic diagnostic beam divergences assuming 5 cm diameter launch and receiver antennae.

5. Signal to noise ratio as a function of diagnostic source peak power with constant energy output of 1 kJ for a CIT scattering diagnostic as described in Table 1. A family of curves is shown for different assumptions in the background signal levels, P_N. Increasing source energy would displace all these curves upward in proportion to the square root of source energy.

6. Millimeter-wave resonances and cutoffs for propagation perpendicular to the magnetic field in the horizontal midplane of tokamaks. The o-mode and upper x-mode cutoffs are not shown.

7. Ray tracing for 200 GHz x-mode propagation in a plasma characteristic of the 10 Tesla compact ignition tokamak with a peak density $6 \times 10^{14} cm^{-3}$.

8. Ray tracing for 200 GHz x-mode propagation in a plasma characteristic of the 10 Tesla compact ignition tokamak with a peak density of $10^{15} cm^{-3}$.

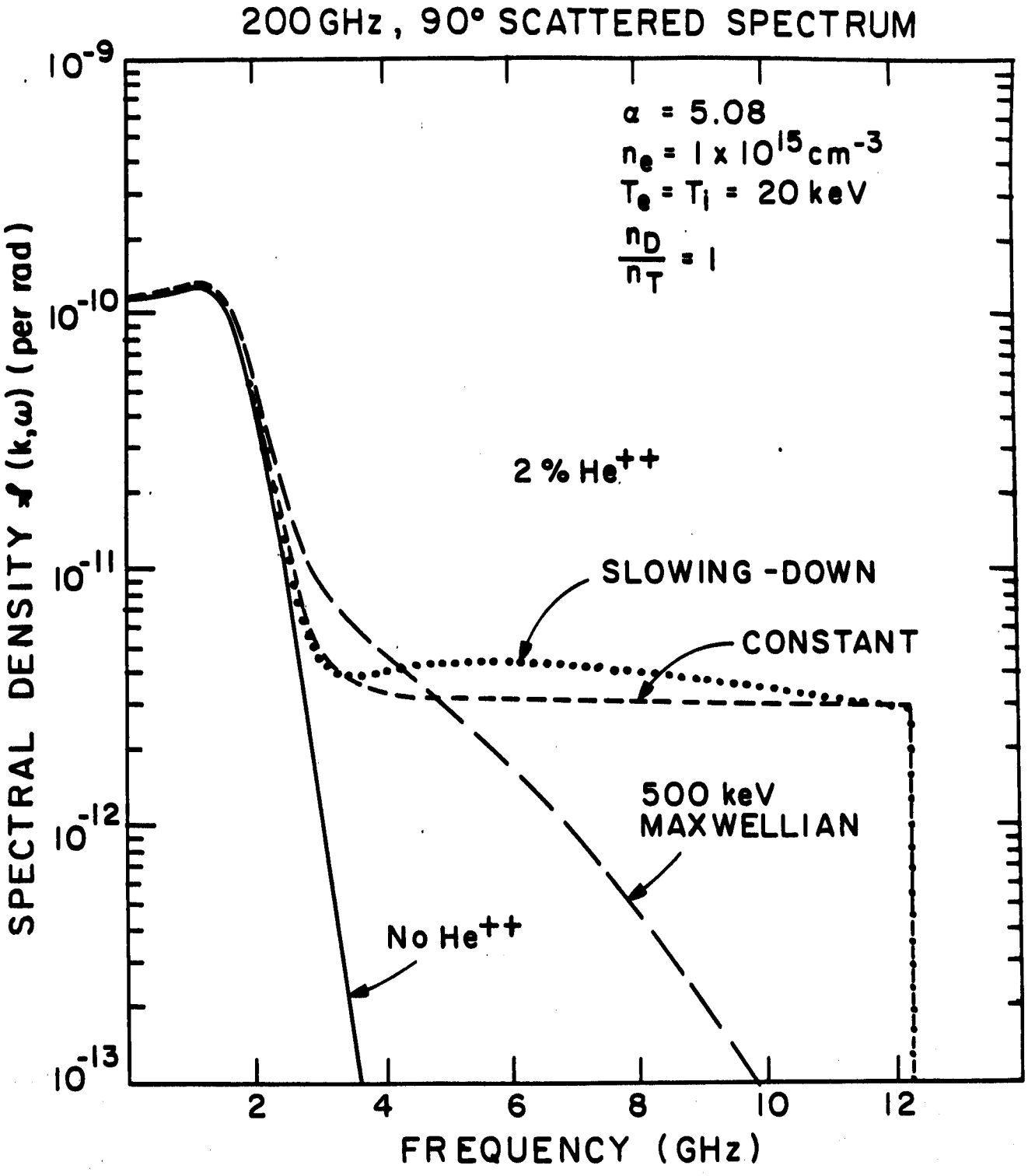
200 GHz, 90° SCATTERED SPECTRUM
α = 5.08
$n_e = 1 \times 10^{15} cm^{-3}$
$T_e = T_i = 20$ keV
$\frac{n_D}{n_T} = 1$
2 % He^{++}
SLOWING-DOWN
CONSTANT
500 keV MAXWELLIAN
No He^{++}
SPECTRAL DENSITY $\mathcal{S}(k,\omega)$ (per rad)
FREQUENCY (GHz)
10^{-9}
10^{-10}
10^{-11}
10^{-12}
10^{-13}
2
4
6
8
10
12

Figure 1

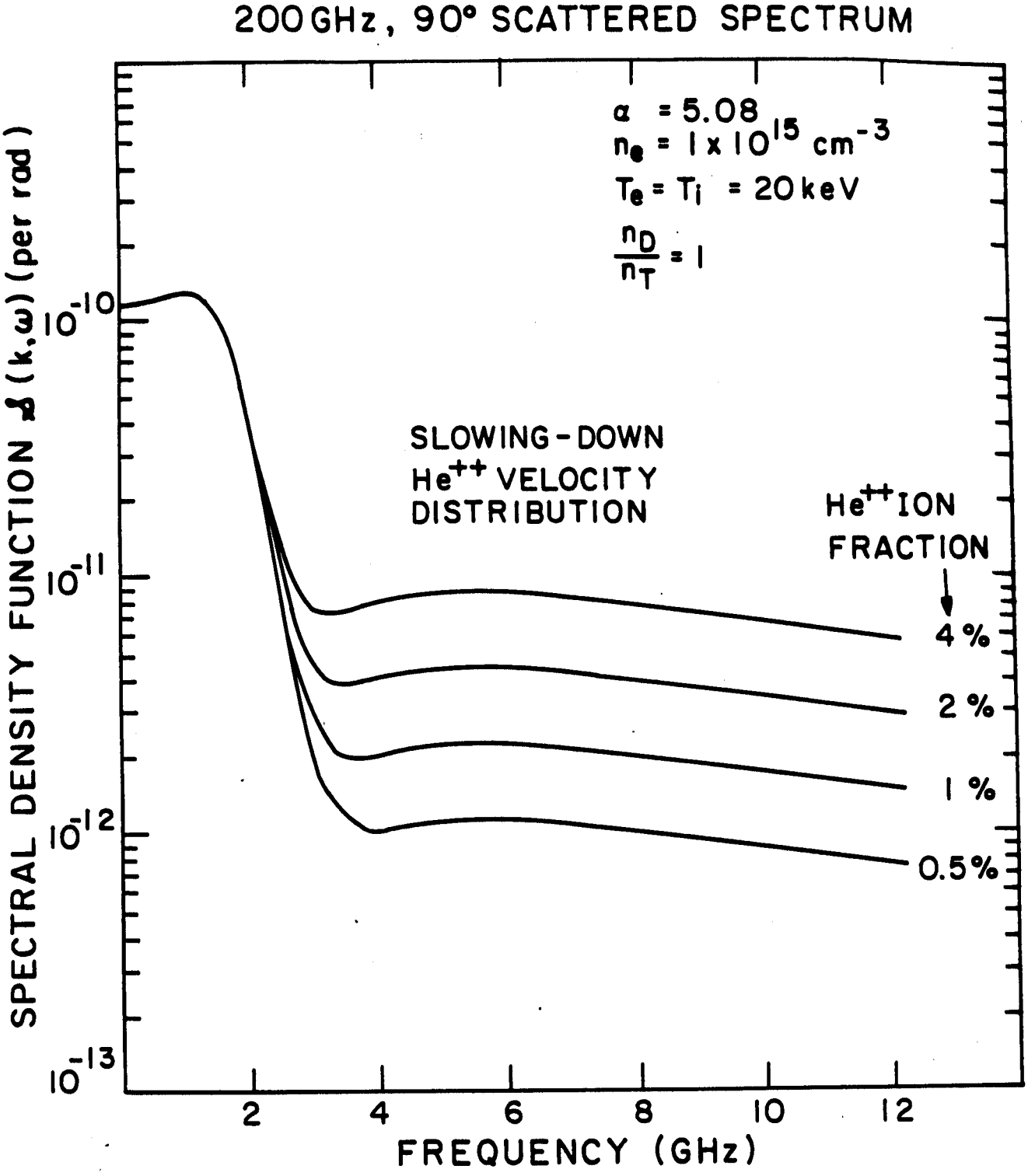
200 GHz, 90° SCATTERED SPECTRUM
α = 5.08
$n_e = 1 \times 10^{15}$ cm^{-3}
$T_e = T_i = 20$ keV
$\frac{n_D}{n_T} = 1$
SLOWING-DOWN
He++ VELOCITY
DISTRIBUTION
He++ ION
FRACTION
4 %
2 %
1 %
0.5 %
SPECTRAL DENSITY FUNCTION $\mathcal{S}(k,\omega)$ (per rad)
10^{-10}
10^{-11}
10^{-12}
10^{-13}
2
4
6
8
10
12
FREQUENCY (GHz)

Figure 2

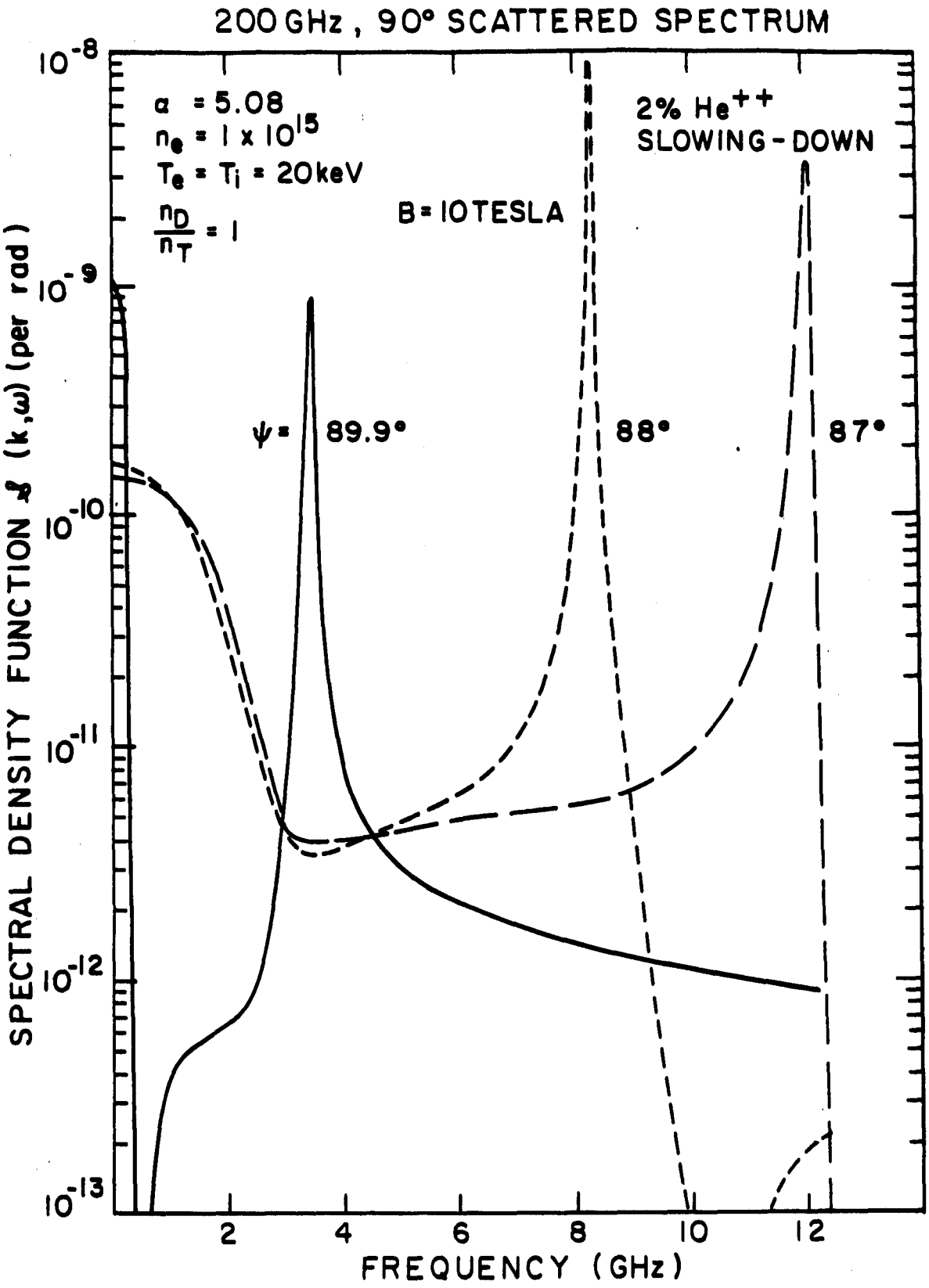
200 GHz, 90° SCATTERED SPECTRUM
α = 5.08
$n_e = 1 \times 10^{15}$
$T_e = T_i = 20keV$
$\frac{n_D}{n_T} = 1$
B = 10 TESLA
2% He^{++}
SLOWING-DOWN
ψ = 89.9°
88°
87°
SPECTRAL DENSITY FUNCTION S (k,ω) (per rad)
10^{-8}
10^{-9}
10^{-10}
10^{-11}
10^{-12}
10^{-13}
2
4
6
8
10
12
FREQUENCY (GHz)

Figure 3

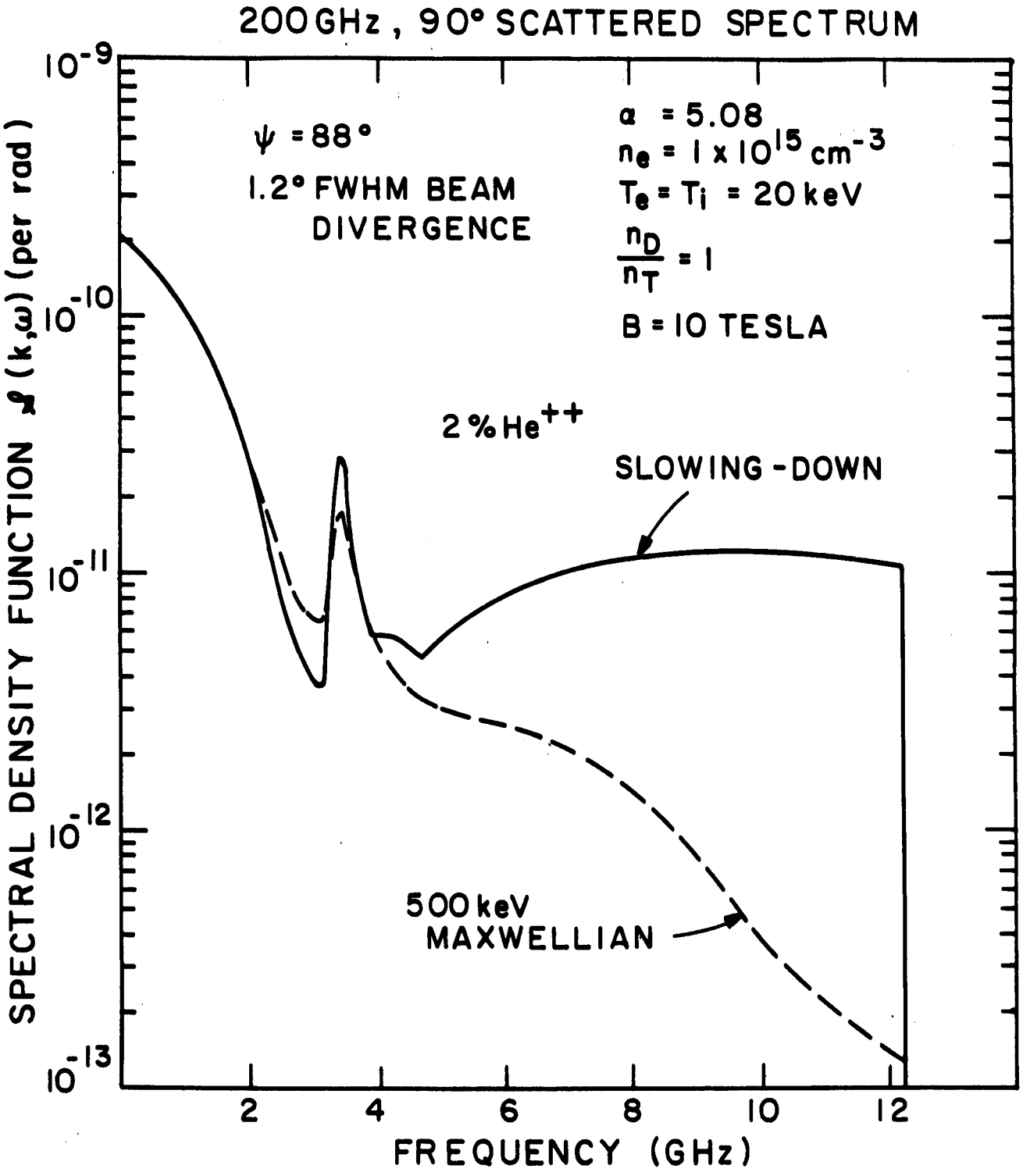
200 GHz, 90° SCATTERED SPECTRUM
ψ = 88°
1.2° FWHM BEAM DIVERGENCE
α = 5.08
$n_e = 1 \times 10^{15}$ cm^{-3}
$T_e = T_i = 20$ keV
$\frac{n_D}{n_T} = 1$
B = 10 TESLA
2% He^{++}
SLOWING-DOWN
500 keV MAXWELLIAN
SPECTRAL DENSITY FUNCTION $\mathcal{S}(k,\omega)$ (per rad)
10^{-9}
10^{-10}
10^{-11}
10^{-12}
10^{-13}
2
4
6
8
10
12
FREQUENCY (GHz)

Figure 4

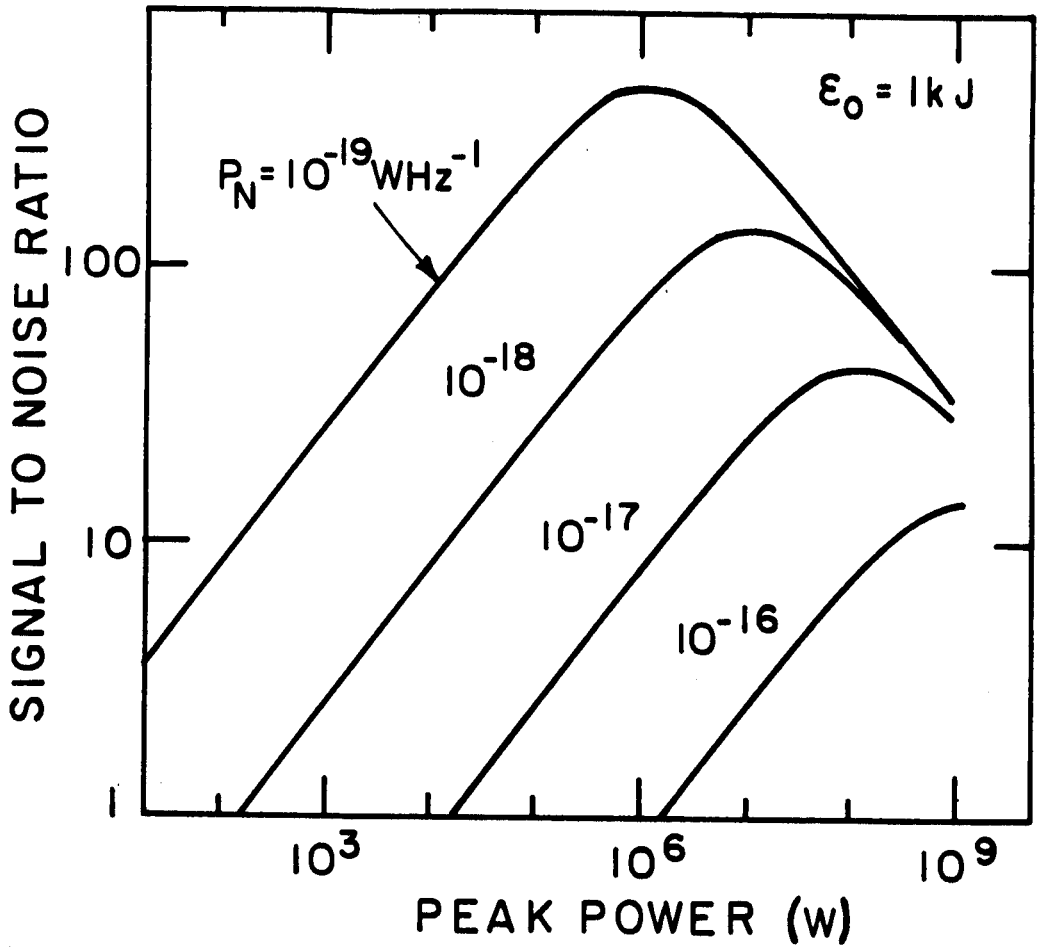
ε_0 = 1kJ
$P_N = 10^{-19} WHz^{-1}$
10^{-18}
10^{-17}
10^{-16}
SIGNAL TO NOISE RATIO
100
10
1
10^3
10^6
10^9
PEAK POWER (W)

Figure 5

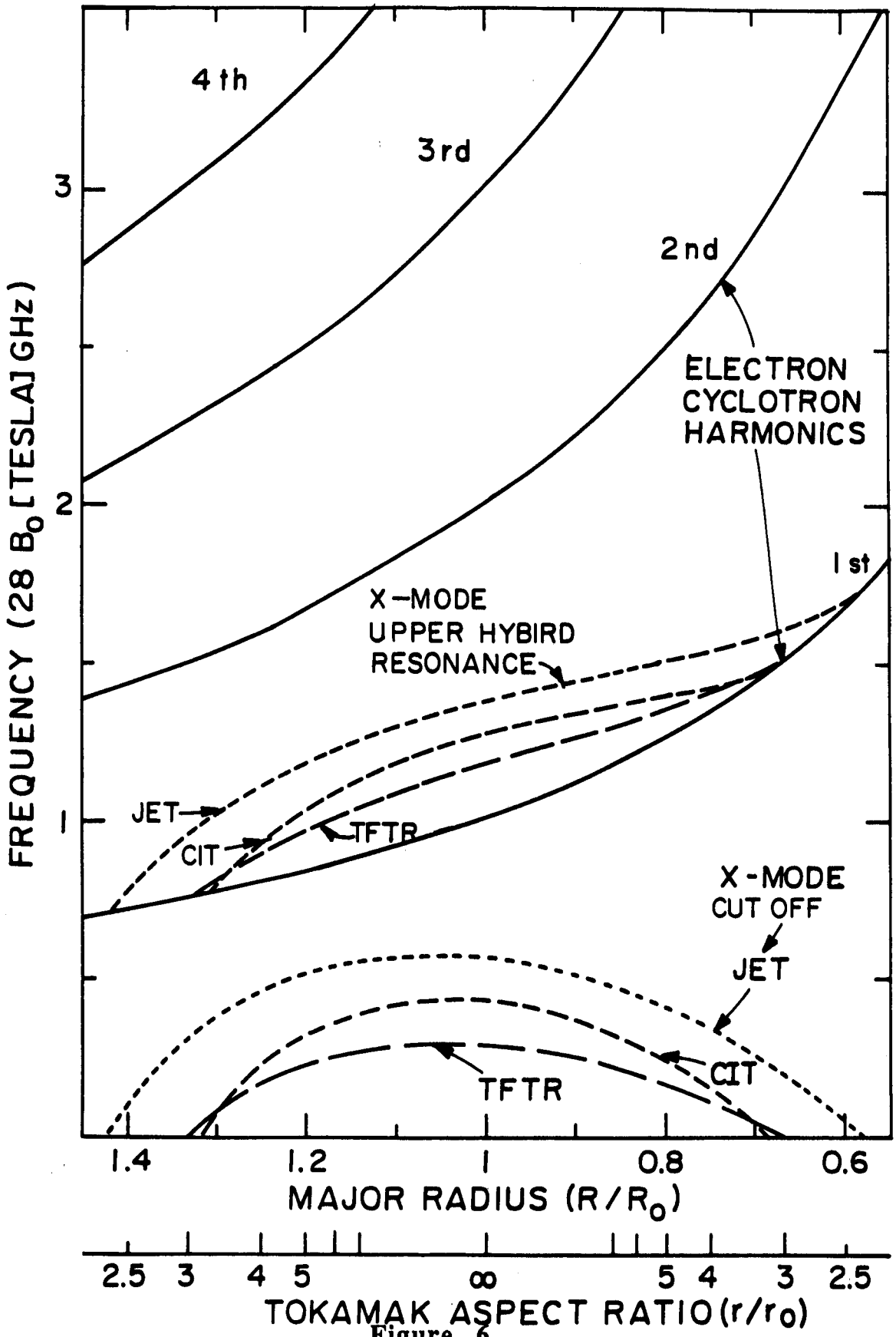
4th
3rd
2nd
1st
ELECTRON
CYCLOTRON
HARMONICS
X-MODE
UPPER HYBIRD
RESONANCE
JET
CIT
TFTR
X-MODE
CUT OFF
JET
CIT
TFTR
FREQUENCY (28 B0 [TESLA] GHz)
3
2
1
1.4
1.2
1
0.8
0.6
MAJOR RADIUS (R/R0)
2.5 3 4 5 ∞ 5 4 3 2.5
TOKAMAK ASPECT RATIO (r/r0)

Figure 6

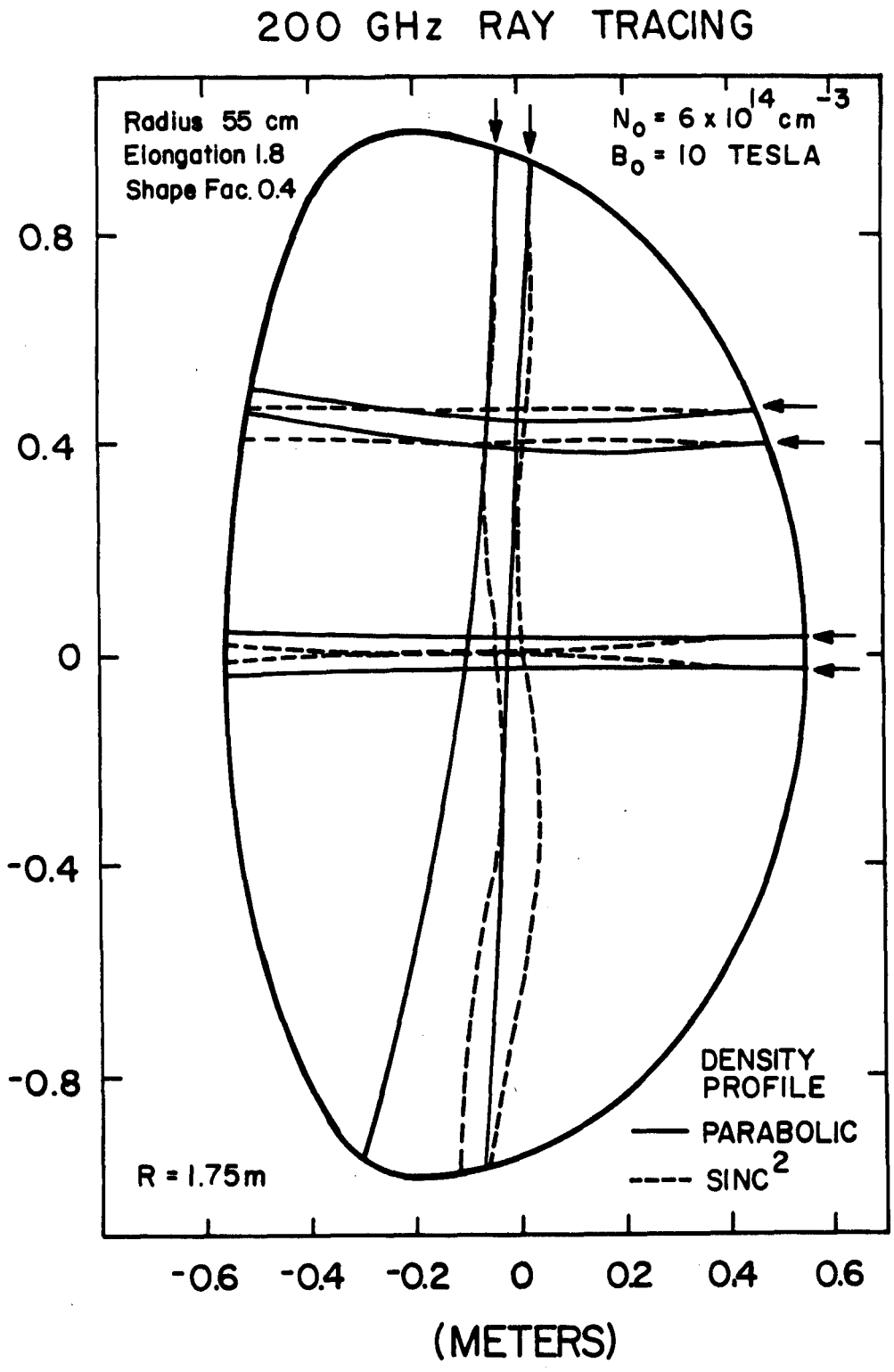
200 GHz RAY TRACING
Radius 55 cm
Elongation 1.8
Shape Fac. 0.4
$N_0 = 6 \times 10^{14}$ cm^{-3}
B_0 = 10 TESLA
0.8
0.4
0
-0.4
-0.8
R = 1.75m
DENSITY PROFILE
PARABOLIC
SINC^2
-0.6 -0.4 -0.2 0 0.2 0.4 0.6
(METERS)

Figure 7

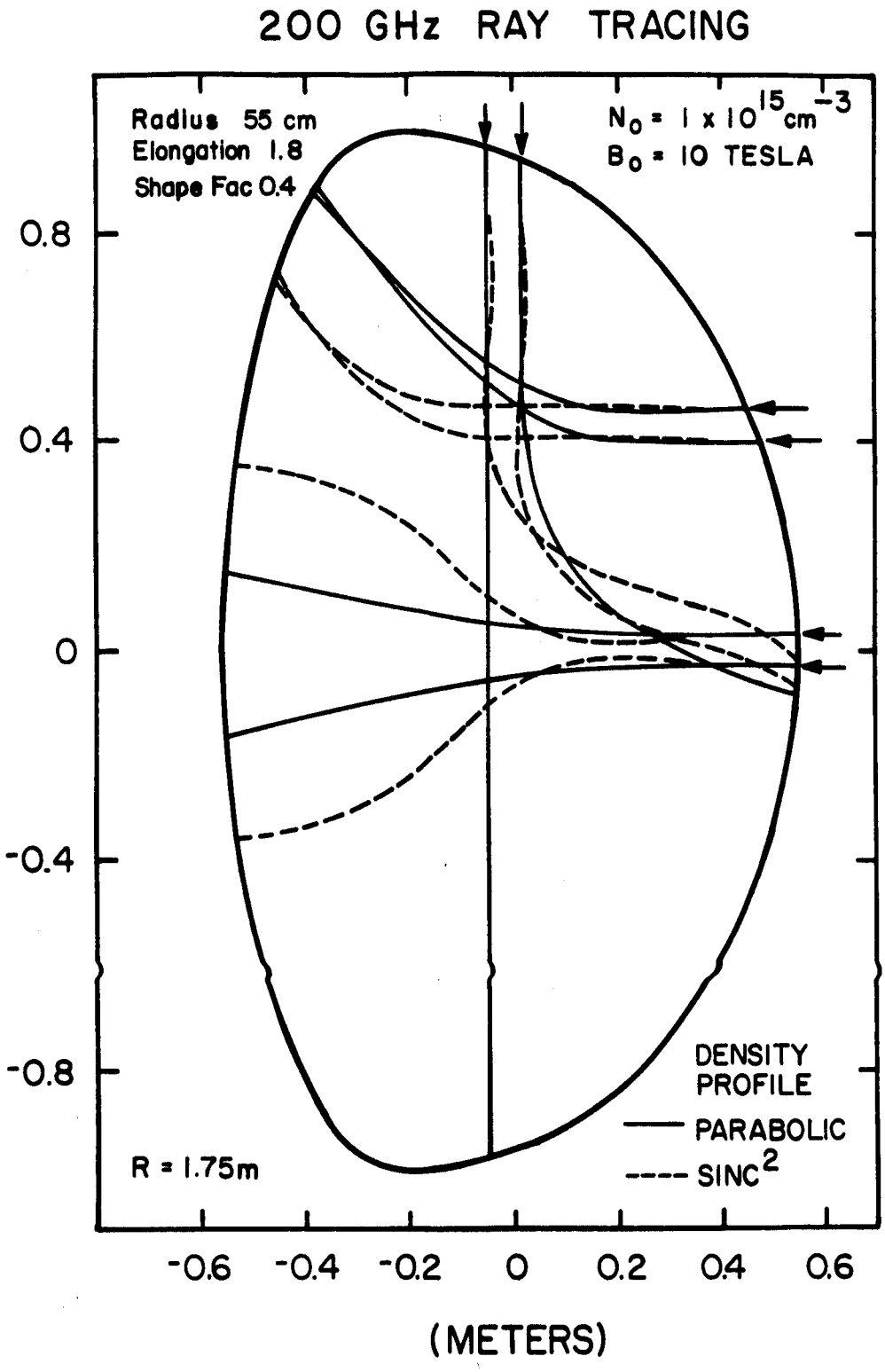
200 GHz RAY TRACING
Radius 55 cm
Elongation 1.8
Shape Fac 0.4
$N_0 = 1 \times 10^{15} cm^{-3}$
$B_0 = 10$ TESLA
0.8
0.4
0
-0.4
-0.8
R = 1.75m
DENSITY PROFILE
PARABOLIC
SINC^2
-0.6 -0.4 -0.2 0 0.2 0.4 0.6
(METERS)

Figure 8